nature nanotechnology

ARTICLES

https://doi.org/10.1038/s41565-017-0003-0

Radiative control of dark excitons at room temperature by nano-optical antenna-tip Purcell effect

Kyoung-Duck Park[1,2,3,4], Tao Jiang[1,2,3,4], Genevieve Clark[5,6], Xiaodong Xu[5,6] and Markus B. Raschke[1,2,3,4]*

Excitons, Coulomb-bound electron–hole pairs, are elementary photo-excitations in semiconductors that can couple to light through radiative relaxation. In contrast, dark excitons (X_D) show anti-parallel spin configuration with generally forbidden radiative emission. Because of their long lifetimes, these dark excitons are appealing candidates for quantum computing and optoelectronics. However, optical read-out and control of X_D states has remained challenging due to their decoupling from light. Here, we present a tip-enhanced nano-optical approach to induce, switch and programmably modulate the X_D emission at room temperature. Using a monolayer transition metal dichalcogenide (TMD) WSe_2 on a gold substrate, we demonstrate ~6×10^5-fold enhancement in dark exciton photoluminescence quantum yield achieved through coupling of the antenna-tip to the dark exciton out-of-plane optical dipole moment, with a large Purcell factor of $\geq2\times10^3$ of the tip–sample nano-cavity. Our approach provides a facile way to harness excitonic properties in low-dimensional semiconductors offering new strategies for quantum optoelectronics.

The 2D nature of monolayer transition metal dichalcogenides (TMDs) creates tightly bound excitons with strong Coulomb interaction and an extraordinarily large binding energy[1–3]. Associated anomalous excitonic properties and strong light–matter interaction suggest a new paradigm for a range of applications in optoelectronics[4–7].

The broken inversion symmetry and strong spin–orbit coupling (SOC) in monolayer TMDs lead to spin- and energy-splitting in the conduction band[8–10]. The electrons with anti-parallel spins in the two respective states of the split conduction band give rise to bright and dark excitons[11–13] by combining with the holes in the higher-lying valence band. These two distinct states of exciton have orthogonal transition dipole orientation associated with the spin configuration, as demonstrated recently both theoretically[10,14] and experimentally at low temperature[15–18].

As known from zero-dimensional quantum dot studies, dark excitons (X_D) have a long lifetime due to solely non-radiative decay channels and spin flip processes[19]. This distinct nature of dark excitons in low-dimensional semiconductors has attracted much attention for potential applications as coherent two-level systems for quantum information processing[20], or Bose–Einstein condensation (BEC)[21], yet a full-scale study is hampered by the out-of-plane transition dipole moments making them difficult to access optically[15–18].

In order to induce radiative emission of dark excitons in atomically thin TMDs, different approaches were demonstrated in recent low temperature photoluminescence (PL) studies. Following a procedure as established for dark exciton emission in quantum dots[22,23], tilting the spin direction by applying a strong external in-plane magnetic field ($\geq$14 T) induces a weakly allowed in-plane optical transition by the Zeeman effect[15,16]. Alternatively, by exciting out-of-plane polarized surface plasmon polaritons (SPP) in a TMD-plasmonic device, radiative X_D emission through dark exciton–SPP coupling can be induced[17]. This weak X_D emission can also be observed through polarization-selective detection from the sample edge[18]. However, these studies have been restricted to cryogenic temperature conditions ($T\leq30$ K), because otherwise the small energy difference of <50 meV between dark and bright exciton leads to thermal excitation into the then overwhelming bright exciton emission channel.

In this work, we demonstrate an approach for dark exciton spectroscopy based on state-selective dark exciton coupling with tip-enhanced PL (TEPL) spectroscopy, as illustrated in Fig. 1a,b. Here, the scanning probe nano-optical antenna-tip selectively couples to the out-of-plane transition dipole moment which facilitates Purcell-enhanced dark exciton emission with few-fs radiative dynamics[24]. With this simple and generalizable approach, we demonstrate excitation, modulation and radiative control of dark exciton emission, at room temperature and with high quantum yield. The combination of the nanoscale localized ($\leq$15 nm) effective excitation through strongly confined out-of-plane optical fields at the tip–Au substrate nano-gap, with antenna-tip mediated near- to far-field mode transformation gives rise to a ~6×10^5-fold X_D-PL enhancement as we demonstrate in monolayer WSe_2 with a Purcell factor $\geq2\times10^3$ enhanced spontaneous emission rate. From precise atomic force microscopy (AFM) nano-gap distance control of the dark exciton to antenna-tip coupling strength, we achieve from simple switching to active modulation of the dark exciton On/Off states in time and space.

Radiative emission of dark excitons at room temperature

The experiment is based on TEPL spectroscopy[25], with side illumination of Au nano-tip manipulated in a shear-force AFM as shown schematically in Fig. 1a (see Methods for details). The Au tip has a normal orientation with respect to a planar Au substrate. TEPL

[1]Department of Physics, University of Colorado, Boulder, CO, USA. [2]Department of Chemistry, University of Colorado, Boulder, CO, USA. [3]JILA, University of Colorado, Boulder, CO, USA. [4]Center for Experiments on Quantum Materials, University of Colorado, Boulder, CO, USA. [5]Department of Physics, University of Washington, Seattle, WA, USA. [6]Department of Materials Science and Engineering, University of Washington, Seattle, WA, USA. *e-mail: markus.raschke@colorado.edu

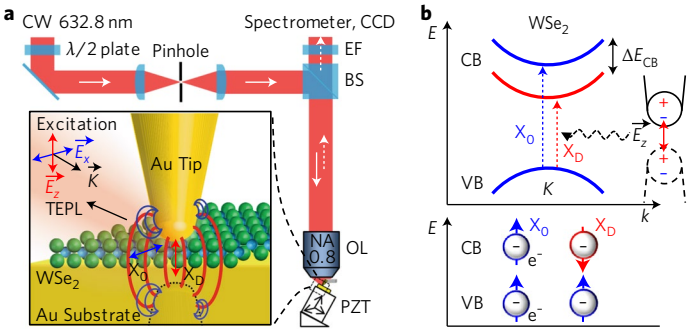

Fig. 1 | Schematic of tip-enhanced photoluminescence spectroscopy and electronic band structure of monolayer WSe_2. a, Selective excitation and probing of the transition dipole moments of dark (out-of-plane) and bright (in-plane) excitons by polarization control. EF, edge filter; BS, beam splitter; OL, objective lens. **b**, Split-band (top) and -spin (bottom) configurations of bright and dark exciton states. Spin-forbidden optical transition of dark excitons is induced by strongly confined local antenna fields with plasmonic Purcell enhancement at the tip-sample nano-gap. CB, conduction band; VB, valence band.

spectroscopy is then performed by tip–sample distance control between the Au tip and a monolayer WSe_2 transferred onto the Au substrate. All experiments are performed at room temperature.

Figure 2a shows TEPL spectra at a 1 nm tip–sample distance with excitation polarization oriented parallel or perpendicular with respect to the sample surface. A strong X_D emission peak is observed (red). In contrast, the X_D response is suppressed for tip-perpendicular polarization (blue) even though an enhanced PL response of X_0 is observed, attributed to an in-plane localized optical field effect in agreement with the spectral X_0 characteristics in far-field emission (black). The difference spectrum after polarization correction for X_0 then corresponds to the pure X_D mode emission (orange). From Lorentzian fitting of the spectra for X_D and X_0, we obtain ~46 meV of intravalley energy splitting between the dark and bright excitons (see Supplementary Fig. 1). This result is in good agreement with recent X_D observations facilitated by in-plane magnetic field (47 meV)[16], SPP coupling (42 meV)[17], and polarization-selective detection from the sample edge (40 meV)[18]. We note that the energy of bright and dark exciton emission is only minimally perturbed by the Au substrate due to the tightly bound excitons within the monolayer (see Supplementary Information for details)[1–3,26]. Further, the TEPL linewidth of the X_D emission is narrower than the bright exciton linewidth, in agreement with previous observation (see Supplementary Fig. 1 for details)[17].

To test for a possible contribution from bi-exciton emission, which has comparable photon energy to dark states, we measure the TEPL intensity as a function of the excitation power for X_D and X_0 emissions. Figure 2b shows the resulting TEPL power dependence based on curve fits to the TEPL spectra and plotting the integrated spectral intensities of X_D and X_0 emissions. On the basis of the linear power dependence behaviour, we exclude bi-exciton emission[27].

To understand the polarization dependence of the X_D emission, and to model the intensity difference of in-plane and out-of-plane local fields at the Au tip–Au substrate junction, we calculate the confined optical field intensity using finite-difference time-domain (FDTD) simulation for our experimental conditions (Fig. 2a). As shown in Fig. 2c,d, in the nano-gap, the optical field intensity of the out-of-plane mode is stronger by a factor of $\geq 3\times10^2$ than that of the in-plane mode, as expected.

For further investigation of the antenna-tip-induced dark exciton emission, we perform TEPL measurements under precise nanometre tip–sample distance control. Figure 3a shows TEPL spectra of monolayer WSe_2 with respect to the distance between the Au tip and Au substrate. Bright exciton emission (X_0) at 1.667 eV is observed in the distance region of 4–12 nm attributed to the enhanced localized (in-plane) near-field excitation at the tip apex. In contrast, for shorter distances, in the 1–3 nm range, dark exciton X_D emission emerges and dominates the spectra at 1.621 eV. In addition, a weak tip-plasmon PL response from the Au–Au nano-gap is seen, as described previously[24]. Figure 3b shows corresponding distance dependence in TEPL intensity for X_D, X_0 and gap plasmon emission. While the X_0 peak intensity saturates below 2 nm distances due to polarization and energy transfer and non-radiative relaxation in the metal tip and substrate, the X_D peak intensity continues to rise sharply, correlated with an increasing gap plasmon PL intensity. Because the in-plane dipole of the X_0 does not couple to the antenna mode, the PL quenching dominates over enhancement at short distances. In contrast, the X_D emission with its out-of-plane dipole, when coupled to the antenna mode with its fs-radiative decay, continues to dominate at short distances[24,28,29].

This behaviour is most clearly evident in the 2D covariance plot (Fig. 3c). From the full data set of Fig. 3a, we calculate the covariance $\sigma(i, j)$ between wavelengths i and j from the distance dependent TEPL intensities $I(i, d)$ using

$$\sigma(i,j)=\frac{1}{N}\sum_{d=d_1}^{d_n}[I(i,d)-\langle I(i)\rangle]\times[I(j,d)-\langle I(j)\rangle] \quad (1)$$

The resulting 2D covariance map clearly shows strong (weak) correlation between the out-of-plane gap plasmon and the dark (bright) exciton emission. The plasmon PL emission serves as an indicator and metric of the X_D-tip polarization transfer and Purcell enhancement of rapid PL emission as established previously (see ref. [24] and following sections for details).

Radiative control of dark excitons

As we demonstrated previously[25], the shear-force AFM tip can also act as an active control element to modify excitonic properties of TMDs both spectrally and spatially. In the optical antenna tip–WSe_2–Au surface configuration, the nano-gap is regulated by a shear-force feedback mechanism[30]. This gives rise to sub-nm precise control of the gap plasmon response, and associated strongly correlated dark exciton emission. Figure 4a–c shows time-dependent spectra of the TEPL response (X_D, X_0 and gap plasmon) during constant (**a**), discrete (**b**), and modulated (**c**) tip–sample distance. The precision of nano-gap control relies on the mechanical quality (Q) factor of the AFM tuning fork. We generally achieve Q-factors of $\geq 4\times10^3$ by attaching two Au tips to both prongs of the tuning fork. Using this high-Q sensor, we regulate a tip–sample distance with ~0.2 nm precision, and stably maintain the X_D On state under ambient conditions with minimal fluctuations (**a**). By varying the distance between 1 nm and 5 nm, the X_D can be switched discretely between its On and Off states (**b**). Correspondingly, by continu-

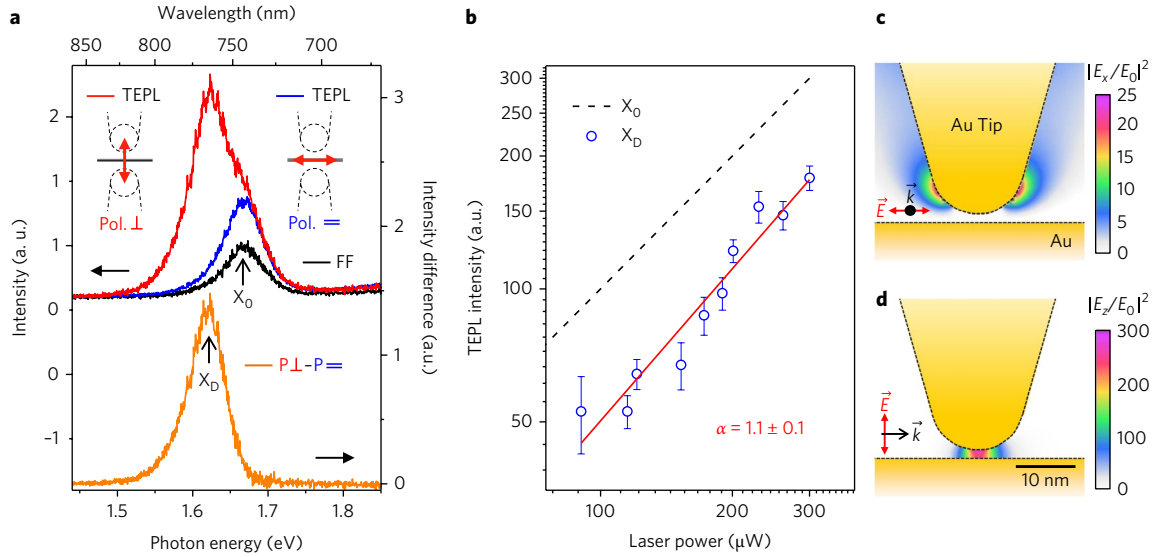

Fig. 2 | Probing radiative emission of dark excitons of monolayer WSe_2 through polarization- and power-dependence of tip-enhanced photoluminescence. a, Excitation polarization dependent TEPL spectra of monolayer WSe_2 on a Au substrate at ~1 nm tip–sample distance with tip-selective X_D emission (orange). **b**, A log-plot of the power dependence of TEPL intensity of dark (X_D) and bright (X_0) excitons. (Red line is a fit of the dark exciton emissions exhibiting a linear power dependence.) **c**,**d**, Finite-difference time domain (FDTD) simulation of the in-plane (**c**) and out-of-plane (**d**) optical field intensity and confinement under the experimental conditions of **a**.

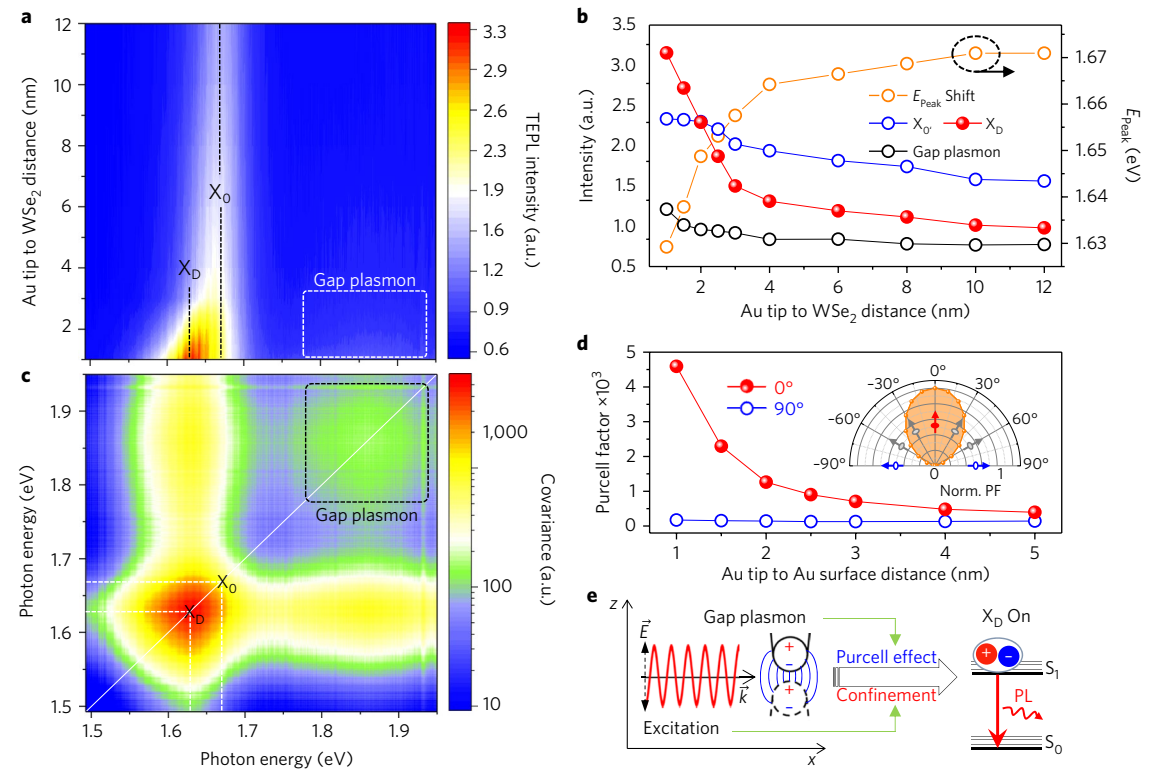

Fig. 3 | Active control of tip-induced radiative emission of dark excitons of monolayer WSe_2. a, Tip–sample distance dependence of TEPL spectra. **b**, Tip–sample distance dependence of peak intensity of TEPL responses (X_D, X_0 and gap plasmon) with spectral energy shift, derived from **a**. **c**, 2D covariance map of the distance dependent TEPL spectra from **a**, exhibiting strong correlation between the gap plasmon and X_D emission. **d**, Simulated plasmonic Purcell factor for out-of-plane and in-plane spontaneous dipole emitters with respect to the distance between the Au tip and Au surface. Inset: normalized plasmonic Purcell factor with respect to emitter orientation. **e**, Illustration of the tip-enhanced emission mechanism of dark excitons as a combination of both enhanced excitation (out-of-plane optical field confinement) and antenna-mediated emission (polarization transfer and enhanced radiative decay by the Purcell effect) at the plasmonic nano-gap.

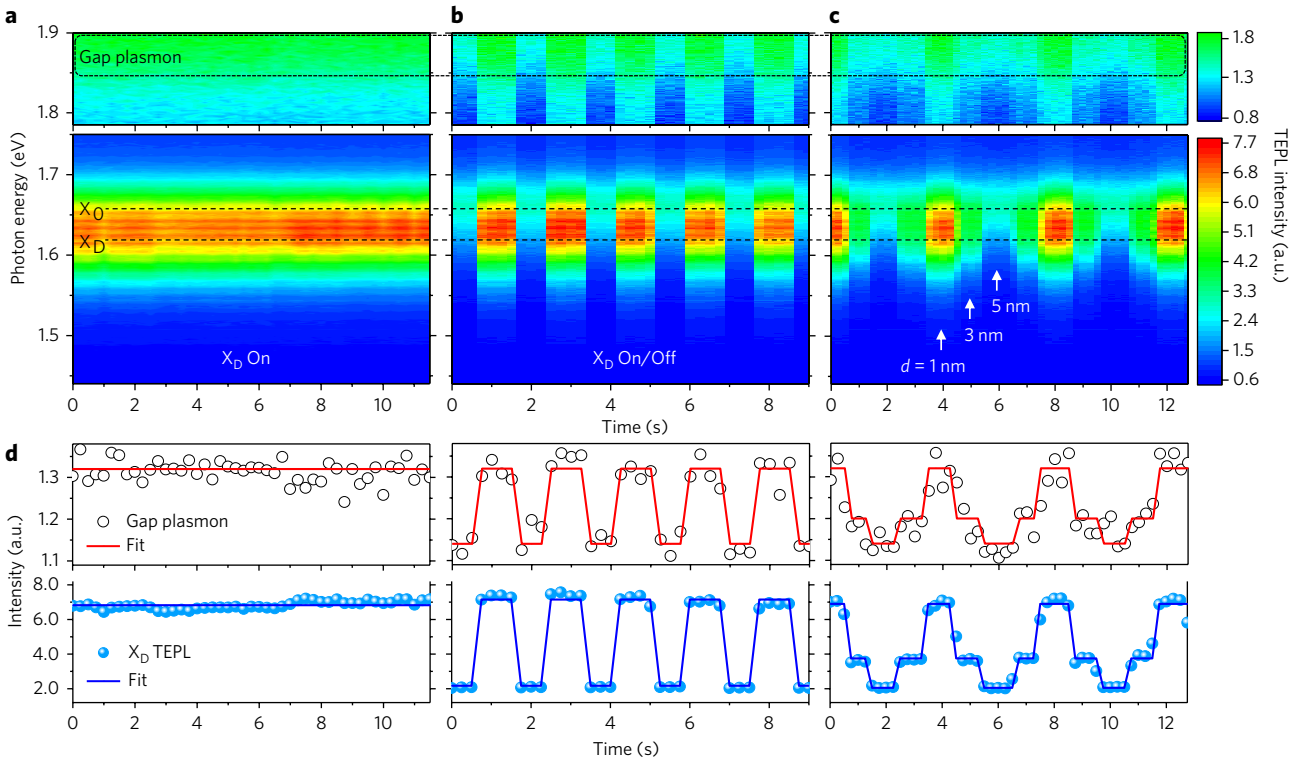

Fig. 4 | Switching and modulation of dark exciton emission. a, Time-series TEPL response (X_D, X_0 and gap plasmon PL) in continuous On state of X_D emission at 1 nm tip–sample distance. **b** Discrete On/Off switching of X_D emission with discrete tip–sample distance variation between 1 nm and 5 nm. **c**, X_D emission modulation by functional control of tip–sample distance. **d**, Time-series of peak intensity of TEPL response with correlation between corresponding X_D emission and gap plasmon, derived from **a**–**c**.

ously time-varying the tip–sample distance, we can programmably modulate the X_D emission (**c**). Figure 4d shows the derived time-series of peak intensity of TEPL response from Fig. 4a–c, with the correlation of X_D PL and gap plasmon verifying the precise control of the X_D emission.

Radiative decay mechanisms of dark excitons

In 2D TMDs, as dictated by the C_{3h} point group and resulting selection rules, only an out-of-plane optical transition is allowed with ~10^{-3}–10^{-2} times smaller radiative decay rate compared with an in-plane optical transition dipole of the bright excitons[10,14,18].

In principle, a spin flip is required to induce radiative decay of the dark excitons[14]. The electron spins can be extrinsically flipped by applying an in-plane magnetic field[16]. Using a large field of ≥14 T, a radiative decay rate $\Gamma \sim 10^{-3}\Gamma_B$ can be obtained with in-plane optical transition by the Zeeman effect[15,16], where Γ_B is the radiative decay rate of the bright excitons. On the contrary, when the mirror symmetry in the surface normal direction is broken (a typical condition for TMD crystals on a flat substrate), an intrinsic spin flip is facilitated by a virtual transition in the conduction band attributed to the SOC mixing. This then induces an out-of-plane dipole transition by the perturbation of a local field[14,31]. Since this transition is between quantum states with identical magnetic quantum number and opposite parity, the transition dipole moments give rise to Bychkov–Rashba coupling to an out-of-plane optical field[32]. The associated radiative decay rate $\Gamma_D \sim (10^{-3}$–$10^{-2})\Gamma_B$ is estimated theoretically[10,14], and is independent of an external field.

In our experimental design, a combination of two physical mechanisms of increase in excitation rate by field enhancement as well as Purcell-factor-induced optical antenna emission (Fig. 3e) is responsible for the ability to detect the dark exciton modes via tip-coupling to an out-of-plane field. First, a strongly confined out-of-plane optical field effectively excites the transition dipole moment of dark excitons with $|E_z|^2$ in the nano-gap enhanced by a factor of $\geq 3\times10^2$ compared to the incident field intensity $|E_0|^2$ (Fig. 2d). In addition, and most significantly, the spontaneous emission rate is enhanced in the nano-gap due to the plasmonic Purcell effect[26,33]. Here, as demonstrated previously[24], near-field dipole–dipole coupling and exciton polarization transfer into the tip with the few-fs radiative lifetime of its plasmonic optical antenna mode, gives rise to an increased emission of the dark exciton with decreasing tip–sample distance. To model this effect we computationally design out-of-plane and in-plane fluorescent model dipole emitters positioned within the nano-gap to calculate the effective Purcell factor ($\gamma_{PF}=\gamma/\gamma_0$, see Supplementary Fig. 2 for details). As shown in Fig. 3d, the Purcell factor of an out-of-plane spontaneous emitter in the tip–surface gap exceeds 2×10^3 for ≤1.5 nm distances as a result of the polarization transfer and rapid radiative tip emission.

Enhancement factor of tip-induced dark exciton emission

For our experimental condition, the resulting overall TEPL intensity enhancement factor (EF) of the dark exciton emission as a combination of both effects given by

$$<EF> = \left|\frac{E_z}{E_0}\right|^2 \times \gamma_{PF} \qquad (2)$$

is estimated to be as high as ~6×10^5 at 1.5 nm plasmonic nano-gap. This enhancement factor of the dark excitons is, to the best of our knowledge, the largest enhancement factor for fluorescent emitters investigated to date. In comparison, even refined plasmonic Ag nanocubes coupled to a Ag film achieved ~3×10^4-fold fluorescence enhancement from cyanine molecules as the closest analogue[33,34].

This extraordinary PL enhancement is due to the strictly out-of-plane oriented transition dipole moment in the atomically thin semiconductor sandwiched in the ≤1.5 nm plasmonic nano-gap.

This out-of-plane mode selective enhancement facilitates the room temperature observation of X_D not readily possible with other techniques. We can quantify the ratio of near-field TEPL intensity of the dark excitons (I_D^{NF}) compared to the far-field PL intensity of the bright excitons (I_B^{FF}) given by

$$\frac{I_D^{NF}}{I_B^{FF}} \approx \left| \frac{E_z}{E_0} \right|^2 \times \gamma_{PF} \times \frac{\Gamma_D}{\Gamma_B} \times \frac{\eta_D}{\eta_B} \quad (3)$$

Here, Γ_D and Γ_B represent respective decay rates, modified by the Purcell factor γ_{PF}, and η_D and η_B are relative occupation numbers of thermally populated dark and bright excitons, respectively, with their ratio η_D/η_B given by $e^{\frac{\Delta E}{k_B T}}$ with ΔE the energy splitting between the dark and bright excitons[35]. With the parameters from above, $I_D^{NF}/I_B^{FF} \sim 4\times10^3 - 4\times10^4$ at 300 K thus facilitates direct probing and active control of the tip-enhanced radiative emission of the dark excitons with strong contrast even at room temperature. In the absence of the antenna-tip polarization and Purcell effect enhancement, the complementary approaches of inducing dark exciton emission by an in-plane magnetic field[15,16], SPP coupling[17], and polarization-selective edge detection[18] do not readily extend to room temperature due to the otherwise dominant spectral weight of the bright exciton.

Conclusion

Our approach thus gives access to potential applications of dark excitons in quantum nano-optoelectronics over a wide temperature range. We envision the demonstrated tip-antenna platform for room temperature dark exciton emission with or without nano-opto-mechnical control[25] as an ideal building block for functional quantum devices. Further, the nanoscale optical switching of the spin states paves the way for new design and fabrication of nano-spintronic devices. Specifically, the control of long-lived dark excitons confined in only ~150 nm^3 mode volume can be exploited to create nanoscale devices for integrated quantum-photonic circuits and active quantum information processors such as nano-light emitting diodes, nano-optical switch/multiplexer, high-density memory and qubits. The nano-confinement further allows for imaging with ≤15 nm spatial resolution of heterogeneity of dark excitonic properties in 2D TMDs[25], with the possibility for an additional modulation in electronic energy with local strain engineering via nano-mechanical tip force control as we demonstrated recently[25]. The range of dynamic controls including coherent ultrafast excitation and tip/antenna manipulation thus gives access to a range of new phenomena at the sub-10 nm scale regime including room temperature strong coupling[36,37], interlayer electron–phonon coupling[38], or out-of-plane exciton behaviours[39]. Further, the range of applications can be extended to dark excitons in semiconducting carbon nanostructures, quantum dots, and molecular materials beyond TMDs and other van der Waals materials.

Methods

Methods, including statements of data availability and any associated accession codes and references, are available at https://doi.org/10.1038/s41565-017-0003-0.

Received: 27 June 2017; Accepted: 15 September 2017;
Published online: 20 November 2017

References

1. Splendiani, A. et al. Emerging photoluminescence in monolayer MoS_2. *Nano Lett.* **10**, 1271–1275 (2010).
2. Mak, K. F., Lee, C., Hone, J., Shan, J. & Heinz, T. F. Atomically thin MoS_2: a new direct-gap semiconductor. *Phys. Rev. Lett.* **105**, 136805 (2010).
3. He, K. et al. Tightly bound excitons in monolayer WSe_2. *Phys. Rev. Lett.* **113**, 026803 (2014).
4. Mak, K. F. & Shan, J. Photonics and optoelectronics of 2D semiconductor transition metal dichalcogenides. *Nat. Photon* **10**, 216–226 (2016).
5. Basov, D., Fogler, M. & de Abajo, F. G. Polaritons in van der Waals materials. *Science* **354**, aag1992 (2016).
6. Tong, Q. et al. Topological mosaics in moire superlattices of van der Waals heterobilayers. *Nat. Phys.* **13**, 356–362 (2017).
7. Hao, K. et al. Direct measurement of exciton valley coherence in monolayer WSe_2. *Nat. Phys.* **12**, 677–682 (2016).
8. Liu, G.-B., Shan, W.-Y., Yao, Y., Yao, W. & Xiao, D. Three-band tight-binding model for monolayers of group-vib transition metal dichalcogenides. *Phys. Rev. B* **88**, 085433 (2013).
9. Kośmider, K., González, J. W. & Fernández-Rossier, J. Large spin splitting in the conduction band of transition metal dichalcogenide monolayers. *Phys. Rev. B* **88**, 245436 (2013).
10. Echeverry, J., Urbaszek, B., Amand, T., Marie, X. & Gerber, I. Splitting between bright and dark excitons in transition metal dichalcogenide monolayers. *Phys. Rev. B* **93**, 121107 (2016).
11. Zhang, X.-X., You, Y., Zhao, S. Y. F. & Heinz, T. F. Experimental evidence for dark excitons in monolayer WSe_2. *Phys. Rev. Lett.* **115**, 257403 (2015).
12. Arora, A. et al. Excitonic resonances in thin films of WSe_2: from monolayer to bulk material. *Nanoscale* **7**, 10421–10429 (2015).
13. Koperski, M. et al. Optical properties of atomically thin transition metal dichalcogenides: observations and puzzles. *Nanophotonics* **6**, 1289–1308 (2017).
14. Slobodeniuk, A. & Basko, D. Spin-flip processes and radiative decay of dark intravalley excitons in transition metal dichalcogenide monolayers. *2D Mater* **3**, 035009 (2016).
15. Molas, M. et al. Brightening of dark excitons in monolayers of semiconducting transition metal dichalcogenides. *2D Mater* **4**, 021003 (2017).
16. Zhang, X.-X. et al. Magnetic brightening and control of dark excitons in monolayer WSe_2. *Nat. Nanotech.* **12**, 883–888 (2017).
17. Zhou, Y. et al. Probing dark excitons in atomically thin semiconductors via near-field coupling to surface plasmon polaritons. *Nat. Nanotech.* **12**, 856–860 (2017).
18. Wang, G. et al. In-plane propagation of light in transition metal dichalcogenide monolayers: optical selection rules. *Phys. Rev. Lett.* **119**, 047401 (2017).
19. Smoleński, T., Kazimierczuk, T., Goryca, M., Wojnar, P. & Kossacki, P. Mechanism and dynamics of biexciton formation from a long-lived dark exciton in a CdTe quantum dot. *Phys. Rev. B* **91**, 155430 (2015).
20. Poem, E. et al. Accessing the dark exciton with light. *Nat. Phys.* **6**, 993–997 (2010).
21. Combescot, M., Betbeder-Matibet, O. & Combescot, R. Bose–Einstein condensation in semiconductors: the key role of dark excitons. *Phys. Rev. Lett.* **99**, 176403 (2007).
22. Nirmal, M. et al. Observation of the 'dark exciton' in CdSe quantum dots. *Phys. Rev. Lett.* **75**, 3728 (1995).
23. Smoleński, T. et al. In-plane radiative recombination channel of a dark exciton in self-assembled quantum dots. *Phys. Rev. B* **86**, 241305 (2012).
24. Kravtsov, V., Berweger, S., Atkin, J. M. & Raschke, M. B. Control of plasmon emission and dynamics at the transition from classical to quantum coupling. *Nano Lett.* **14**, 5270–5275 (2014).
25. Park, K.-D. et al. Hybrid tip-enhanced nanospectroscopy and nanoimaging of monolayer WSe_2 with local strain control. *Nano Lett.* **16**, 2621–2627 (2016).
26. Wang, Z. et al. Giant photoluminescence enhancement in tungsten-diselenide–gold plasmonic hybrid structures. *Nat. Commun.* **7**, 11283 (2016).
27. You, Y. et al. Observation of biexcitons in monolayer WSe_2. *Nat. Phys.* **11**, 477–481 (2015).
28. Kühn, S., Håkanson, U., Rogobete, L. & Sandoghdar, V. Enhancement of single-molecule fluorescence using a gold nanoparticle as an optical nanoantenna. *Phys. Rev. Lett.* **97**, 017402 (2006).
29. Anger, P., Bharadwaj, P. & Novotny, L. Enhancement and quenching of single-molecule fluorescence. *Phys. Rev. Lett.* **96**, 113002 (2006).
30. Park, K.-D. et al. A new method of *Q* factor optimization by introducing two nodal wedges in a tuning-fork/fiber probe distance sensor. *Rev. Sci. Instrum.* **81**, 093702 (2010).
31. Bychkov, Y. A. & Rashba, E. I. Oscillatory effects and the magnetic susceptibility of carriers in inversion layers. *J. Phys. C Solid State Phys.* **17**, 6039 (1984).
32. Ochoa, H. & Roldán, R. Spin-orbit-mediated spin relaxation in monolayer MoS_2. *Phys. Rev. B* **87**, 245421 (2013).
33. Akselrod, G. M. et al. Probing the mechanisms of large purcell enhancement in plasmonic nanoantennas. *Nat. Photon.* **8**, 835–840 (2014).
34. Rose, A. et al. Control of radiative processes using tunable plasmonic nanopatch antennas. *Nano Lett.* **14**, 4797–4802 (2014).

35. Crooker, S., Barrick, T., Hollingsworth, J. & Klimov, V. Multiple temperature regimes of radiative decay in CdSe nanocrystal quantum dots: intrinsic limits to the dark-exciton lifetime. *Appl. Phys. Lett.* **82**, 2793–2795 (2003).
36. Chikkaraddy, R. et al. Single-molecule strong coupling at room temperature in plasmonic nanocavities. *Nature* **535**, 127–130 (2016).
37. Kleemann, M.-E. et al. Strong-coupling of WSe_2 in ultra-compact plasmonic nanocavities at room temperature. Preprint at https://arxiv.org/abs/1704.02756 (2017).
38. Jin, C. et al. Interlayer electron-phonon coupling in WSe_2/hBN heterostructures. *Nat. Phys.* **13**, 127–131 (2017).
39. Rivera, P. et al. Valley-polarized exciton dynamics in a 2D semiconductor heterostructure. *Science* **351**, 688–691 (2016).

Acknowledgements

The authors would like to thank M. D. Lukin for insightful discussions. K.-D.P., T.J. and M.B.R. acknowledge funding from the US Department of Energy, Office of Basic Sciences, Division of Material Sciences and Engineering, under award no. DE-SC0008807. G.C. and X.X. acknowledge support from NSF-EFRI-1433496. We also acknowledge support provided by the Center for Experiments on Quantum Materials (CEQM) of the University of Colorado.

Author contributions

M.B.R. and K.-D.P. conceived the experiment. K.-D.P. performed the measurements and the FDTD simulations. K.-D.P. and M.B.R. designed the samples, and G.C. and X.X. prepared the samples. K.-D.P. and M.B.R. analysed the data, and all authors discussed the results. K.-D.P. and M.B.R. wrote the manuscript with contributions from all authors. M.B.R. supervised the project.

Competing interests

The authors declare no competing financial interests.

Additional information

Supplementary information is available for this paper at https://doi.org/10.1038/s41565-017-0003-0.

Reprints and permissions information is available at www.nature.com/reprints.

Correspondence and requests for materials should be addressed to M.B.R.

Publisher's note: Springer Nature remains neutral with regard to jurisdictional claims in published maps and institutional affiliations.

Methods

Sample preparation. WSe_2 monolayers are grown by physical vapour transport using powdered WSe_2 as precursor material. Source material (30 mg) in an alumina crucible is placed in the hot zone of a 25.4 mm horizontal tube furnace, and an SiO_2 substrate is placed downstream in a cooler zone at the edge of the furnace (750–850 °C). Before growth, the tube is evacuated to a base pressure of 0.13 mbar and purged several times with argon. The furnace is then heated to 970 °C at a rate of 35 °C per min and remains there for a duration of 5–10 min before cooling to room temperature naturally. A flow of 80 SCCM argon and 20 SCCM hydrogen is introduced as carrier gas during the 5–10 min growth period. The as-grown WSe_2 crystals are then transferred onto flat template stripped Au substrates using a wet transfer technique. For that purpose, PMMA (6% in anisole) is spin-coated onto the SiO_2 wafer, covering the region with WSe_2 monolayer crystals. The wafer is then placed in a solution of dilute hydrofluoric acid (20% in distilled water), until the SiO_2 layer is etched away and the PMMA membrane with WSe_2 crystals floats free. The membrane is then rinsed in distilled water to remove residual etchant, and scooped up onto a wire loop. The PMMA membrane can then be placed onto the Au substrates under an optical microscope, similar to the commonly used dry transfer technique. Once the membrane has been lowered into contact with the substrate, heating the substrate ≥160 °C melts the PMMA layer releasing it from the wire loop.

TEPL spectroscopy setup. In the TEPL spectroscopy setup, the sample is mounted to a piezoelectric transducer (PZT, P-611.3, Physik Instrumente) with sub-nm precision positioning. Electrochemically etched Au tips (~10 nm apex radius) are attached to a quartz tuning fork (resonance frequency = ~32 kHz)[25]. To regulate the tip–sample distance, the AFM shear-force amplitude is monitored and controlled from the electrically driven tuning fork[40]. Coarse tip positioning is performed using a stepper motor (MX25, Mechonics AG), and shear-force feedback and sample position are controlled by a digital AFM controller (R9, RHK Technology). The sample surface is tilted by ~60° with respect to the incident *k*-vector for effective excitation. A helium–neon laser beam (632.8 nm, ≤0.3 mW), after passing through a half wave plate for polarization control, is focused into the junction between the Au substrate and the tip apex by an objective lens (NA = 0.8, LMPLFLN100×, Olympus). TEPL signal is collected in the backscattered direction, passed through an edge filter (633 nm cut-off) and detected using a spectrometer (f = 500 mm, SpectraPro 500i, Princeton Instruments) with a thermoelectrically cooled, electron-multiplied, charge-coupled device (CCD, ProEM+: 1600 eXcelon3, Princeton Instruments). The spectrometer is calibrated using hydrogen and mercury lines, and a 150 grooves per mm grating is used to obtain a high bandwidth spectrum for simultaneous measurement of gap plasmon and TEPL spectra.

Data availability. The data that support the plots within this paper and other findings of this study are available from the corresponding author upon reasonable request.

References

40. Karrai, K. & Grober, R. D. Piezoelectric tip-sample distance control for near field optical microscopes. *Appl. Phys. Lett.* **66**, 1842–1844 (1995).